IEEE Access
Multidisciplinary ⋮ Rapid Review ⋮ Open Access Journal

Received 19 April 2022, accepted 6 June 2022, date of publication 14 June 2022, date of current version 8 July 2022.

Digital Object Identifier 10.1109/ACCESS.2022.3183154

Dynamic Local Path Planning for Intelligent Vehicles Based on Sampling Area Point Discrete and Quadratic Programming

HAOBIN JIANG[1], JIAN PI[2], AOXUE LI[2], AND CHENHUI YIN[2]
[1]Automotive Engineering Research Institute, Jiangsu University, Zhenjiang 212013, China
[2]School of Automotive and Traffic Engineering, Jiangsu University, Zhenjiang 212013, China

Corresponding author: Haobin Jiang (jianghb@ujs.edu.cn)

This work was supported in part by the Key University Science Research Project of Jiangsu Province under Grant 16KJA58001.

ABSTRACT This paper proposes a dynamic path planning method based on discrete optimization applied to suburban highways or expressways. We optimize the generated candidate points according to the cost function and then generates a local path through the quintic spline curve. The kinematics and obstacle boundary conditions are set up to improve the reliability of the planned path. Meanwhile, the two-dimensional normal distribution obstacle cost function, comfort cost function and acceleration cost function are designed to evaluate candidate points and speed. Various types of roads scenes, including dynamic and static obstacles, such as straight roads, S- bend, are established to verify the method's feasibility. The simulation shows that the method can efficiently avoid various obstacles and plan an ideal path that complies with traffic laws.

INDEX TERMS Intelligent vehicles, local path planning, dynamic planning, cost function, discrete optimization.

I. INTRODUCTION

With the development of artificial intelligence and Internet communication technology, intelligent vehicles have gradually become popular. Compared with traditional vehicles, intelligent vehicles have considerable advantages in safety, efficiency and comfort [1], it has taken a centre stage in the automotive industry in recent years [2].

The research on intelligent vehicles focuses on four modules: perception, planning, decision-making and control [3]. Path planning is one of these four core modules, and it can be divided into two levels. The high-level named global planning, in this level, global routes and the vehicle states are determined from a digital map and localization system [4]. The bottom layer is local path planning. It can be defined as real-time planning of the vehicle's transition from one feasible state to the next while satisfying the vehicle's kinematic limits based on vehicle dynamics and constrained by occupant comfort, lane boundaries and traffic rules, while, at the same time, avoiding obstacles [5]. In a dynamic and complex environment or under dynamic constraints, local path planning plays a vital role in the safety of intelligent vehicles [6].

The current studies on path planning can be divided into three categories: traditional path planning methods (A* star, artificial potential field, etc.), learning algorithms and dynamic planning algorithms.

The most representative traditional path planning algorithms include A* algorithm and artificial potential field algorithm. The A* algorithm is improved from Dijkstra's algorithm [7]. It builds grid cells on the environment to find the globally optimal path connecting the initial position of each cell to the target position while also avoiding obstacles. The A* algorithm has been used in many scenarios. In 2007' DARPA Urban Challenge (DUC), many teams used the A* algorithm to implement automated driving [8]. Artificial potential field method is widely used in path planning of small robot collision avoidance systems such as drones [9]. The basic idea is to construct the repulsion field of the obstacle and the gravitational field of the target, and a path can then be achieved along the steepest gradient of the potential field. On the basis of the traditional artificial potential field algorithm, Wu EM proposed an improved artificial potential field algorithm using the backtracking-filling method to solve

The associate editor coordinating the review of this manuscript and approving it for publication was Razi Iqbal.

the local minima problem, and achieved success in the field of motion robots [10]. The traditional path planning algorithm has the advantages of simplicity and high efficiency, but the path is easy to fall into the local optimum, and it is not suitable for the complex and high-speed actual road environment where the vehicle travels.

Topical and highly influential research direction, machine learning is gradually being applied to the field of path planning. Machine learning is designed to allow vehicles to have the ability to learn independently rather than rigidly following established procedures [11]. Reinforcement learning is one of the typical representatives of machine learning, has been applied to different path planning environments in recent years. Zhao *et al.* combines asynchronous methods with existing tabular reinforcement learning algorithms, to propose a parallel architecture to solve the discrete space path planning problem [12]. Kim *et al.* used an inverse reinforcement learning algorithm to solve socially adaptive path planning in a dynamic environment [13]. Reinforcement learning can allow vehicles to solve unexpected problems in actual situations autonomously and can adapt to complex scenarios as well, but requires extensive training, poor reliability, and high hardware requirements, thus the path planning algorithm based on reinforcement learning only stays at the experimental level and has not yet been used in real vehicles.

Dynamic programming is a mathematical method to solve the optimization of the multi-stage decision-making process. In recent years, it has come under much attention in intelligent vehicle path planning, which is an effective methods to solve the problem of path planning [14]. Baidu Apollo nomancar adopts the EM planning [15] and lattice planning [16] based on dynamic programming in path planning, which have received much attention in literature. Feng proposed improved dynamic window algorithm, which performs real-time dynamic planning through discrete speeds, makes the robot have a tremendous obstacle avoidance ability [17]. Jiang present a robust autonomous driving dynamic trajectory planning method in urban environments, which successfully avoided dynamic and static obstacles through trajectory refinement, trajectory interpolation [18]. Compared with traditional path planning algorithms, dynamic programming has excellent real-time performance and a powerful ability to deal with discrete problems, and it can adapt to complex and changeable road environments [19]. Compared with the path planning algorithm based on machine learning, dynamic planning has low hardware requirements, and has been successfully deployed in actual vehicles.

This paper designs a dynamic path planning method for intelligent vehicles based on discrete optimization, which can be effectively applied to local path planning in suburban highways or expressways. The method firstly examines the driving condition according to vehicle and road information, generating discrete sampling points according to different driving conditions. Then establish boundary conditions to constrain the sampling area of candidate points. Finally, a quadratic programming algorithm is used to optimize the cost function to obtain the best position of the vehicle at the next moment and connect it to the vehicle's current position using a quintic spline curve. According to the road environment, the method is iterated every 0.2 seconds; each time a path is generated, the vehicle drove within 2 seconds. Finally, an ideal local path is planned. This method fully considers the impact of dynamic and static obstacles when establishing boundary conditions, and constructs a cost function that is more suitable for the road scene. Compared with dynamic path planning based on path discretization, such as state lattice planning [20], this method can efficiently and reliably plan reasonable local paths and speeds in various complex road environments.

The rest of the paper is organized as follows: Section II introduces the method of generating candidate points, Section III explains the process of establishing the boundary conditions, Section IV describes how to quadratic program on the cost function of candidate points to generate the optimal path, Section V gives the simulation results, and Section VI is the conclusion of the paper.

II. CANDIDATE POINTS GENERATION

A. INFORMATION CLASSIFICATION

The location of obstacles has a more significant impact on the planned path. According to the form of movement, obstacles in our method can be divided into static obstacles and dynamic obstacles. Static obstacles refer to obstacles with a speed less than 1m/s^2, and the vice versa are dynamic obstacles. Obstacles can be divided into forward obstacles and side obstacles according to the relative position. We stipulate with a lateral distance less than $|\Delta l|$ from the vehicle are forward obstacles, and those with a lateral distance greater than $|\Delta l|$ are lateral obstacles, where $\Delta l = \pm 1.5$ m. The type of obstacle will affect the boundary conditions and cost function. The information required for local path planning in our method is known. High-precision maps provide road information, obstacles and vehicles information is obtained from on-board sensors.

B. COORDINATES CONVERSION

Due to the diversity and complexity of the road alignment, it is very strenuous to make the road discretization by only adopting the inertial x-y coordinate [21]. In order to improve the calculation efficiency, our method uses the s-l coordinate system to describe the shape of the road.

The s-l coordinate system is the arc length-offset coordinate system. As shown in Fig. 1, where s represents the arc length along the centre line, and l represents the lateral offset of the centre line [22].

In this paper, candidate points and candidate paths are generated based on the s-l coordinate. The sensors, high-precision maps and path tracking control are based on the Cartesian coordinate. Consequently, conversion between coordinate systems is required. In our method, the discrete projection method is used to transform the coordinate.

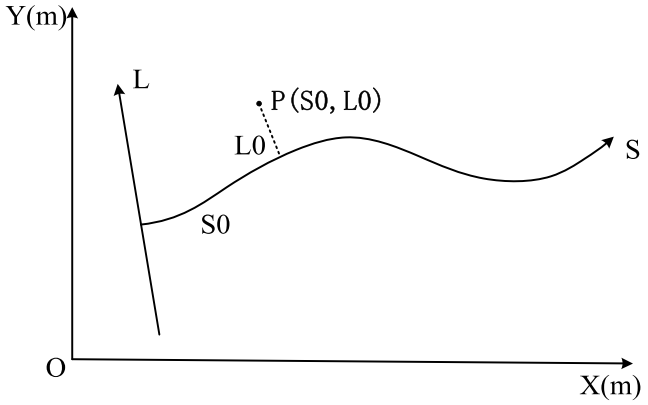

FIGURE 1. s-l coordinate.

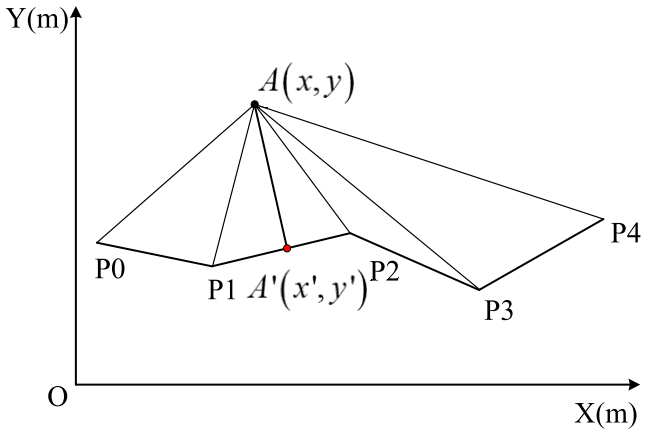

FIGURE 2. Conversion of the cartesian coordinate to the s-l coordinate.

This method avoids complex integral calculations and enhances the real-time performance of the planning algorithm.

The conversion of the Cartesian coordinate to the s-l coordinate is shown in Fig.2. The centerline of the road is discretized into multiple line segments, and the points to be converted are projected onto the discrete line segments. After finding the line segment where the projection point is located, the s and l coordinates can be obtained according to the geometric relationship:

$$\begin{aligned} s &= |P_1P_2| + \ldots + |P_{i-1}P_i| + \left|P_iA'\right| \\ l &= \left|AA'\right| \end{aligned} \tag{1}$$

where A is the conversion point; A' is the projection point; $|P_{i-1}P_i|$ is the length of the discrete line segment; $\left|AA'\right|$ is the distance from the conversion point to the projection point.

The conversion of the s-l coordinate to the Cartesian coordinate adopts the method in Chen *et al.* [23]. As shown in Fig.3, project the conversion point to the centre line of the road. According to the geometric relationship, the Cartesian coordinates of the point can be obtained as:

$$\begin{cases} x_d = x_r + l_d \cdot \cos\theta \\ y_d = y_r + l_d \cdot \sin\theta \end{cases} \tag{2}$$

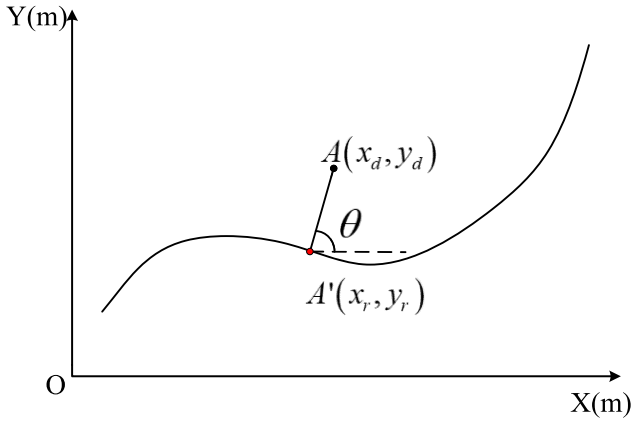

FIGURE 3. Conversion of the s-l coordinate to the cartesian coordinate.

TABLE 1. The minimum safe following distance.

speed range (v_0)	minimum safe following distance
>100km/h	100m
50~100km/h	v_0m
20~50km/h	$0.8v_0$m
<20km/h	$0.5v_0$m

where x_d, y_d are the Cartesian coordinates of the conversion point A; x_r, y_r are the Cartesian coordinates of the projection point $A^{'}$; l_d is the l coordinate of the conversion point; θ is the angle between the $AA^{'}$ and the x-axis in the counterclockwise direction, where $\theta \in [0, 2\pi]$.

C. JUDGMENT OF DRIVING CONDITIONS

In the traditional discrete optimization path planning method, any condition applies the same method to generate candidate points or candidate paths, which will increase the amount of calculation when the vehicle is only driving along the centre line. Consequently, our method divides the driving conditions of the vehicle into starting conditions, cruise conditions, obstacle-avoidance conditions and adjustment conditions to generate candidate points. The switching mode between various driving conditions is shown in Fig. 4.

In starting conditions, the vehicle will accelerate at a constant acceleration until the speed reaches the cruising speed. We take the starting acceleration $a_s = 2\text{m/s}^2$.

In cruising conditions, the vehicle will travel along the lane centre at cruising speed. The cruising speed v_c will be determined according to the speed limit of the lane, In our method, the carriageway takes $v_c = 0.8\ v_{lr}$, and the overtaking lane take $v_c = 0.9\ v_{lr}$. Where v_{lr} is the speed limit of the current lane.

Obstacle-avoidance conditions triggered when the distance between the vehicle and the forward obstacle is less than the safe following distance. The minimum safe following distance recommended by Yimer *et al.* [24] is shown in the Table 1.

In adjustment conditions, the vehicle will accelerate or decelerate at a constant adjusted acceleration. We take the adjustment acceleration $a_j = 1\text{m/s}^2$.

D. GENERATE CANDIDATE POINTS

Candidate sampling points refer to a series of points generated by all feasible end positions of the vehicle after driving for 2 seconds. The candidate points are generated according to the driving conditions of the vehicle in the following two methods.

1) NON-OBSTACLE AVOIDANCE CONDITIONS

Non-obstacle avoidance conditions only generate a candidate point in the direction of the vehicle along the coordinate s, and the candidate point should satisfy (3)

$$\begin{cases} s_e = \begin{cases} s_s + v_0 t_e + \frac{1}{2} a_s t_e^2 \\ s_s + v_c t_e \\ s_s + v_0 t_e \pm \frac{1}{2} a_{acc} t_e^2 \end{cases} \\ l_e = l \end{cases} \tag{3}$$

where *i*, *ii*, and *iii* represent starting conditions, cruise conditions and adjustment conditions; s_s and l_s are the starting point coordinates of the vehicle; s_e and l_e are the coordinates of the candidate points; v_0 is the initial vehicle speed; t_e is the planned interval time, where $t_e = 2\text{s}$.

2) OBSTACLE AVOIDANCE CONDITIONS

Obstacle avoidance conditions will generate a series of candidate points in a sampling area, and coordinates of these candidate points should satisfy (4).

$$\begin{cases} s_{ei} = s_{l\,\text{lim}} + i \cdot 0.1 \quad |s_{l\,\text{lim}}| \le s_{ei} \le |s_{u\,\text{lim}}| \\ \qquad i = 1, 2, \cdots, m \\ l_{ej} = l_{l\,\text{lim}} + j \cdot 0.1 \quad |l_{l\,\text{lim}}| \le l_{ej} \le |l_{u\,\text{lim}}| \\ \qquad \text{j} = 1, 2, \cdots, n \end{cases} \tag{4}$$

where s_{ei} and l_{ej} are the coordinates of the candidate planning points, totalling $i \times j$; m and n are the number of vertical and horizontal candidate points; $s_{u\text{lim}}$ and $s_{l\text{lim}}$ are the upper and lower boundaries of the sampling area, where the upper boundary is the s coordinate of the end point after the vehicle accelerates along the centre of the lane for 2s with the limited maximum acceleration $a_{u\text{lim}}$, considering that the acceleration per 100 meters of a general passenger car is about 2.8m/s^2, in our method, $a_{u\text{lim}}$ is taken as 2.5m/s^2; the lower boundary is the s coordinate of the end point after the vehicle decelerates along the centre line of the lane for 2s with the limited minimum acceleration $a_{l\text{lim}}$, taking into account the braking comfort, the maximum braking deceleration should not be greater than 2.5m/s^2, for comprehensive safety consideration, the value of $a_{u\text{lim}}$ is taken as $-3\ \text{m/s}^2$, $s_{u\text{lim}}$ and

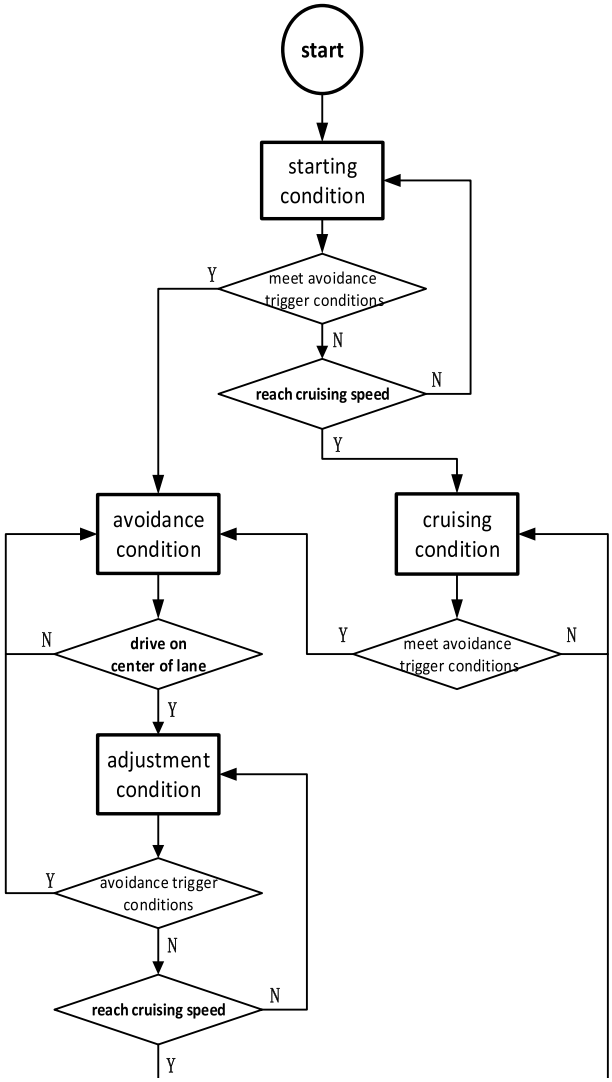

FIGURE 4. Switching process of each driving condition.

$s_{l\text{lim}}$ can be calculated by (5).

$$\begin{cases} s_{u\,\text{lim}} = s_s + v_0 t_e + \frac{1}{2} a_{u\,\text{lim}} t^2 \\ s_{l\,\text{lim}} = s_s + v_0 t_e + \frac{1}{2} a_{l\,\text{lim}} t^2 \end{cases} \tag{5}$$

$l_{u\text{lim}}$ and $l_{l\text{lim}}$ are the left and right boundaries of the sampling area, which is the l coordinate of the road boundary. In our method, the width of a single lane is set to 3.5m, consequently $l_{u\text{lim}} = 3.5\text{m}$ and $l_{l\text{lim}} = -3.5\text{m}$.

Since there is only one candidate point for non-obstacle avoidance conditions, only the candidate points for obstacle avoidance conditions need to be optimally selected.

III. ESTABLISH BOUNDARY CONDITIONS

The vehicle should drive along the planned path safely, stably and under traffic regulations. Therefore, vehicle kinematics and dynamic boundary conditions need to be set to constrain the sampling area of candidate points. In addition, to reduce

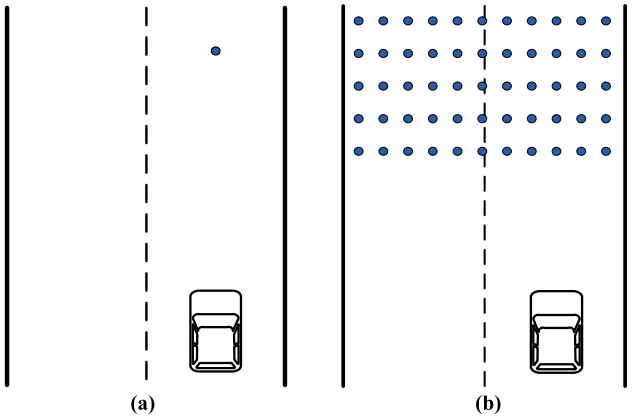

FIGURE 5. Candidate point generation. (a) candidate point of non-obstacle avoidance conditions, (b) candidate point of obstacle avoidance conditions.

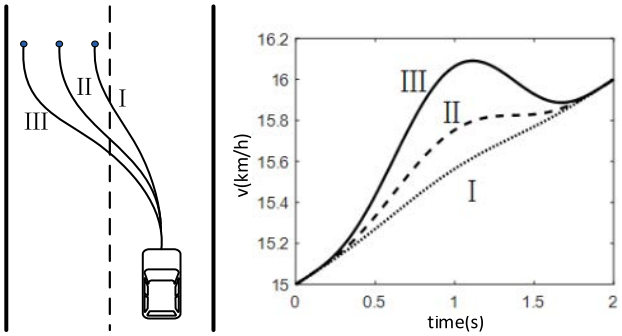

FIGURE 6. The vehicle speed under different lateral displacements when candidate points have the same longitudinal displacement.

the risk of planned collision and improve the reliability of the planned path, this paper sets obstacle boundary conditions to constrain the sampling area of candidate points further.

A. LATERAL ACCELERATION BOUNDARY CONDITIONS

The excessive lateral acceleration of the vehicle will cause the tire cornering stiffness to drop sharply, and tire cornering behaviours will enter into the instability region, the vehicle will have risks such as sideslip [25]. The lateral acceleration a_l of the vehicle shall meet the following requirements:

$$a_l \leq a_{l\max} \tag{6}$$

where a_{lmax} is the maximum lateral acceleration of the vehicle without instability. On a well-adhered road surface $a_{lmax} = 0.4\text{g}$.

The lateral acceleration of the vehicle is divided into the offset lateral acceleration and the centripetal acceleration. The offset lateral acceleration refers to the lateral acceleration generated when the vehicle moves in the l direction, and the road curvature generates the centripetal acceleration. The lateral acceleration a_l of the vehicle can be calculated by (7).

$$a_l = \begin{cases} a_d + a_c, & \text{sgn}(k_d) = \text{sgn}(k_c) \\ a_d - a_c, & \text{sgn}(k_d) \neq \text{sgn}(k_c) \end{cases} \tag{7}$$

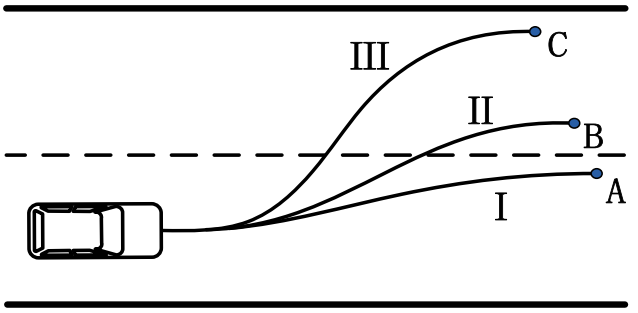

FIGURE 7. Path under the same arc length and different lateral displacement.

where a_d is the offset lateral acceleration; a_c is the centripetal acceleration; k_d is the curvature of the planned path; k_c is the road curvature, when k_d and k_c are in the same direction, a_l is the combination of the offset lateral acceleration and the centripetal acceleration, on the contrary, it is the difference between the offset lateral acceleration and the centripetal acceleration.

The offset lateral acceleration at time t is the second derivative of the vehicle displacement equation in the l direction:

$$a_d = \ddot{l} \tag{8}$$

The quintic spline curve constructs the displacement equation in the l direction:

$$l = \alpha_1 t^5 + \alpha_2 t^4 + \alpha_3 t^3 + \alpha_4 t^2 + \alpha_5 t + \alpha_6 \tag{9}$$

It satisfies the boundary conditions:

$$\begin{cases} l(0) = l_s, \quad \dot{l}(0) = v_{ls}, \quad \ddot{l}(0) = a_{ls} \\ l(t_e) = l_g, \quad \dot{l}(t_e) = 0, \quad \ddot{l}(0) = 0 \end{cases} \tag{10}$$

where v_{ls} and a_{ls} are the lateral velocity and acceleration of the vehicle's initial position; l_s is the l coordinate of the vehicle's initial position; v_{ls}, a_{ls} and l_s are all known quantities; α_i is the polynomial coefficient; l_g is the l coordinate of any candidate point.

The centripetal acceleration at time t can be calculated by (11).

$$\begin{cases} a_c = \dfrac{v_{sg}}{\rho} \\ v_{sg} = v_0 + t^2 \dfrac{(s_g - v_0 t_e)}{t_e^2} \end{cases} \tag{11}$$

where v_{sg} is the longitudinal speed of the vehicle at time t; ρ is the road curvature radius at time t; s_g is the s coordinate of any candidate point.

Simultaneous (7)-(11), solving inequality (6) can get the left/right limit value of l_g at any s coordinate $l_{g\max i}/l_{g\min i}$.

According to (12), we can obtain the left/right boundary l_{llater}/l_{rlater} that satisfies the lateral acceleration constraint.

$$\begin{cases} l_{llater} = \max[l_{g\min 1}, l_{g\min 2}, \cdots, l_{g\min i}] \\ l_{rlater} = \min[l_{g\max 1}, l_{g\max 2}, \cdots, l_{g\max i}] \end{cases} \tag{12}$$

B. ROAD SPEED LIMIT BOUNDARY CONDITIONS

When the vehicle is driving on the planned path, the speed cannot exceed the speed limit of the lane. Therefore, the planned vehicle speed v_{car} should meet:

$$v_{car} \leq v_{\lim} \tag{13}$$

where v_{lim} is the maximum speed limit of the lane.

We assume that the acceleration of the vehicle in the s direction is constant, and the displacement equation in the s direction can be obtained as:

$$\begin{cases} s = s_s + v_0 t + \dfrac{1}{2} a_{long} t^2 \\ a_{long} = 2 \cdot \dfrac{s_g - v_0 t_e}{t_e^2} \end{cases} \tag{14}$$

where s_g is the s coordinate of any candidate point, which is an unknown quantity; a_{long} is the longitudinal acceleration required for the vehicle to reach the candidate point s_g in time t_e.

The displacement equation in the l direction can also be expressed by (9). It can be seen from Fig.6 that the instantaneous lateral velocity is related to the lateral offset. The instantaneous maximum lateral velocity of the planned path occurs when the lateral deviation is the largest, and the new boundary conditions can be obtained:

$$\begin{cases} l(0) = l_s, \quad \dot{l}(0) = v_{ls}, \quad \ddot{l}(0) = a_{ls} \\ l(t_e) = l_{v\max}, \quad \dot{l}(t_e) = 0, \quad \ddot{l}(0) = 0 \end{cases} \tag{15}$$

where

$$l_{v\max} = \max[|l_{llater}|, |l_{rlater}|].$$

Simultaneous (9)(14)(15), according to the principle of extreme value, we can obtain the instantaneous maximum velocity $v_{car'}$ when travelling along the path with the endpoint coordinate l_{vmax}:

$$v_{car'}(t_{\max}, s_g) = \sqrt{\dot{s}^2 + \left(\frac{\partial l}{\partial t}\right)^2} \tag{16}$$

where $t_{\max}$ is the time to reach the maximum instantaneous velocity, and its solution has two situations in the interval [0, 2]: a. $v_{car'}$ has and only one extreme point falls within the interval [0, 2]; b. $v_{car'}$ extreme point fall out of the interval [0, 2]. For case a, $t_{\max}$ is the extreme point of $v_{car'}$ falling in the interval [0, 2]; for case b, $t_{\max} = 2$s.

Incorporating (16) to solve inequality (13), the upper boundary of the road speed limit s_{vlim} can be solved.

C. VEHICLE ACCELERATION BOUNDARY CONDITIONS

In 2.4, when solving the upper bound s_{ulim} of the sampling area, it is assumed that the vehicle has no lateral offset. The planned path potential being a lateral offset. As shown in Fig.7, It has the same average acceleration when the vehicle drives along the same arc length path I, II, III. It is not difficult to find that the larger the lateral offset of the sampling point, the smaller the end position s coordinate that the vehicle can reach, accordingly the path with the minor end position s coordinate needs to satisfy (15).

The arc length L_{road} of any planned trajectory needs to meet:

$$L_{road} \leq L \tag{17}$$

where L is the distance that the vehicle accelerates at 2.5m/s^2 for 2s.

Simultaneous (9)(14)(15), the equation of planning path l concerning s can be obtained:

$$l = f(s) \tag{18}$$

When the vehicle is travelling at 2.5m/s^2, its path arc length can be calculated by (19):

$$L_{road} = \int_{s_s}^{s_{long\,\lim}} \sqrt{1 + \dot{l}^2(s)} \tag{19}$$

where $s_{long\lim}$ is the upper boundary of vehicle acceleration.

Simultaneous (17)-(19), we can obtain the upper boundary of vehicle acceleration $s_{long\lim}$.

D. OBSTACLE BOUNDARY CONDITIONS

To further improve the safety and reliability of the planned path, in addition to using the cost function to evaluate the obstacles, additional boundary conditions of the obstacles need to be established to constrain the sampling area. Obstacle boundary conditions include forward obstacle boundary conditions and lateral obstacle boundary conditions.

This paper introduces the S-T map when analyzing the boundary conditions of obstacles. The S-T map is a two-dimensional relationship diagram of the longitudinal displacement and time of a given local path [26]. Each obstacle and the planned path will produce a projection on the S-T map. If the obstacle projection and the path projection intersect on the S-T map, it indicates a risk of collision with the obstacle when the vehicle is driving along the path.

Forward obstacles have different constraints on the forward lane and the lateral lane. For the forward lane, the distance in the s direction between the candidate point and the forward obstacle should be less than the Minimum Following Distance (MFD). MDF refers to the minimum distance that a vehicle can safely stop within a specific range from the front vehicle when the front vehicle suddenly brakes or has stationary obstacles. This paper adopts the fitting formula of the MDF proposed by the reference [27]:

$$\text{MDF} = 0.0029\,(v \times 3.6)^2 + 0.3049\,(v \times 3.6) \tag{20}$$

where v is the vehicle speed.

From (21), the boundary condition of the forward obstacle to the forward lane can be obtained as:

$$s_{conm12} = s_{locend} - \text{MDF} \tag{21}$$

where s_{conm12} is the upper boundary of the forward lane constrained by the forward obstacle; s_{locend} is the s coordinate after the forward obstacle drives at a constant speed for 2s.

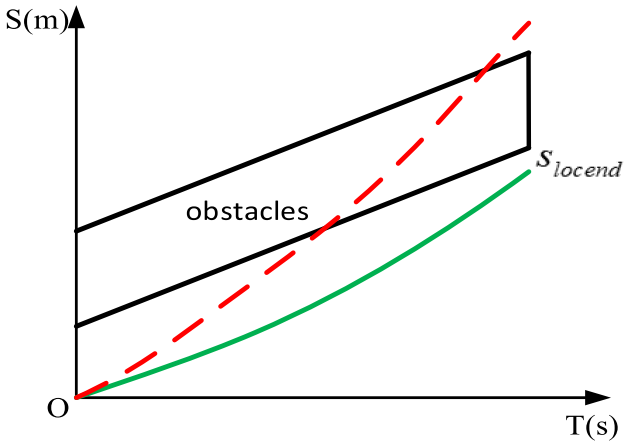

FIGURE 8. The S-T map of forward obstacles and the planned path.

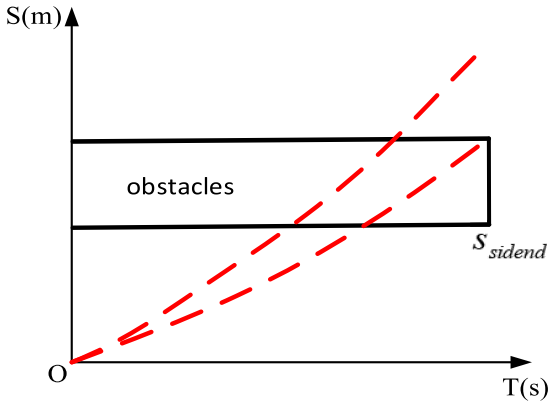

FIGURE 9. The S-T map of the path projection and obstacle projection when the lateral obstacles are static.

For lateral lanes, it is necessary to ensure that the vehicle avoids collisions with forward obstacles during lane changing. The S-T Map of forward obstacles and the planned path is shown in Fig.8.

It can be seen from Fig.8 that when the endpoint coordinate s_g of the vehicle is greater than the end point coordinate s_{sidend} of the forward obstacle, the obstacle projection must intersect the path projection. consequently, the coordinates of the candidate point should meet:

$$s_g \leq s_{locend} \tag{22}$$

When $s_g = s_{locend}$, the s coordinate of the candidate point $s_{conm22} = s_g$ is the upper boundary of the lateral lane constrained by the forward obstacle.

The lateral obstacle boundary condition only constrains the lateral lane, and it can be divided into the following three situations:

1) THE LATERAL OBSTACLES ARE STATIC & THE LATERAL OBSTACLES ARE DYNAMIC, AND THE INITIAL POSITION IS PARALLEL TO THE VEHICLE

In these two cases, the S-T Map of the planned path projection and obstacle projection that the planning vehicle may drive through is shown in Fig.9 and Fig.10.

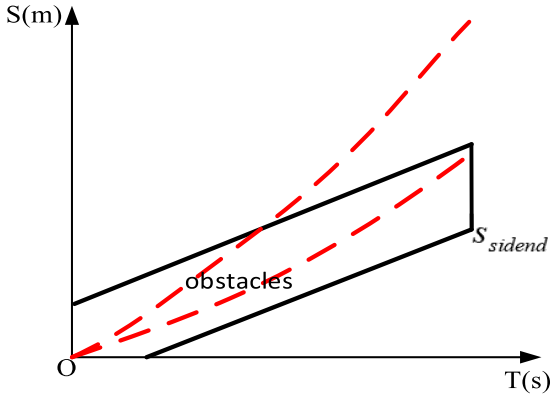

FIGURE 10. The S-T map of the path projection and obstacle projection when the lateral obstacles are static.

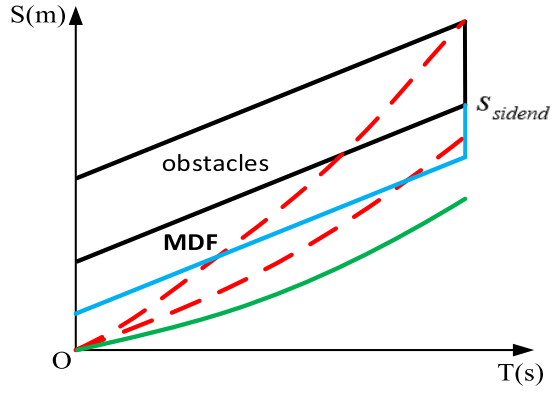

FIGURE 11. The S-T map of the path projection and obstacle projection when the lateral obstacles are dynamic and the initial position in front of the planned vehicle.

It can be seen from Fig.9 and Fig.10 that all possible path projections intersect with obstacle projections or cannot maintain a sufficiently safe distance from the obstacle at the endpoint. In these two cases, the sampling area located in the lateral lane is not feasible.

2) THE LATERAL OBSTACLES ARE DYNAMIC, AND THE INITIAL POSITION IN FRONT OF THE PLANNED VEHICLE

In this case, the S-T Map of the path projection and obstacle projection that the vehicle may drive through is shown in Fig.11.

It can be seen from Fig.11 that when the endpoint coordinate s_g of the vehicle is smaller than the endpoint coordinate s_{sidend} of the lateral obstacle, the path projection will not intersect the obstacle projection. In order to maintain a sufficiently safe distance from the lateral obstacles after lane changing, the MDF needs to be considered. Therefore, the boundary conditions of the lateral obstacle, in this case, should meet:

$$s_{sidem22} = s_{sidend} - \text{MDF} \tag{23}$$

where $s_{sidem22}$ is the upper boundary of the lateral lane constrained by the lateral obstacle; s_{sidend} is the s coordinate after the lateral obstacle drives at a constant speed for 2s.

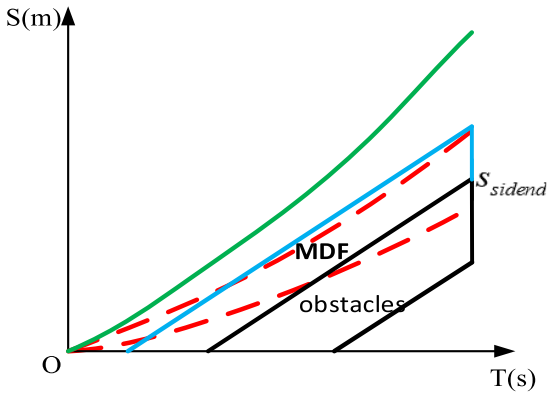

FIGURE 12. The S-T map of the path projection and obstacle projection when the lateral obstacles are dynamic, and the initial position is behind the planned vehicle.

3) THE LATERAL OBSTACLES ARE DYNAMIC, AND THE INITIAL POSITION IS BEHIND THE PLANNED VEHICLE

In this case, the S-T Map of the path projection and obstacle projection that the vehicle may drive through is shown in Fig.12.

It can be seen from Fig.12 that when the endpoint coordinate s_g of the vehicle is greater than the endpoint coordinate s_{sidend} of the lateral obstacle, the path projection will not intersect the obstacle projection. At the same time, the MDF should be considered. In this case, the boundary conditions of the lateral obstacle should meet:

$$s_{sidem21} = s_{sidend} + \text{MDF} \tag{24}$$

where $s_{sidem21}$ is the lower boundary of the lateral lane constrained by lateral obstacles.

Combining the above boundary conditions, the total boundary conditions can be obtained by (25).

$$\begin{cases} s_{11} = s_{llim} \\ s_{12} = \min[s_{ulim}, s_{vlim}, s_{longlim}, s_{conm12}] \\ s_{21} = \max[s_{llim}, s_{sidem21}] \\ s_{22} = \min[s_{ulim}, s_{vlim}, s_{longlim}, s_{conm22}, s_{sidem22}] \\ l_1 = \max[l_{llim}, l_{llater}] \\ l_2 = \min[l_{ulim}, l_{rlater}] \end{cases} \tag{25}$$

where s_{11} and s_{12} are the lower and upper boundaries of the sampling area of the forward lane; s_{21} and s_{22} are the lower and upper boundaries of the sampling area of the lateral lane; l_1 and l_2 are the left and right boundaries of the sampling area.

Our method evaluates the obstacle avoidance safety and comfort of each candidate point and its generated path by designing a cost function, at the same time uses the cost function to influence the speed decision of the vehicle when lane changing.

TABLE 2. The minimum safe following distance.

Lane and obstacle information		Speed planning
No vehicle in lateral lanes	Overtaking lane	Acceleration
	Carriageway	Deceleration
Vehicles in front of the lateral lanes	Lateral lane vehicle slower	Determined by the type of lane
	Lateral lane vehicle faster	Deceleration
Vehicles in front of the lateral lanes	Lateral lane vehicle faster	Determined by the type of lane
	Lateral lane vehicle slower	Deceleration

IV. CANDIDATE POINTS OPTIMIZATION AND PATH GENERATION

A. DESIGN COST FUNCTION

1) OBSTACLE COST FUNCTION

The obstacle cost function includes forward obstacle cost function, lateral obstacle cost function and road cost function.

The road cost function should consider the influence of the boundaries and marking lines stipulated by traffic laws. In a standard two-lane road, the lane centre should have the lowest cost; the road boundary and the double yellow line should have the highest cost. In addition, vehicles passing the lane line to avoidance are allowed. Therefore, the cost of the lane line should not be too high [28]. Thus the ideal shape of the road cost function should be W-shaped, which can be expressed by the fourth-degree polynomial constructed by equation (26).

$$F_{road} = af \left(l_g - 1.5\right)^2 \left(l_g + 1.5\right)^2 \tag{26}$$

where F_{road} is the road cost; af is the road influence coefficient; l_g is the l coordinate of any point in the sampling area.

The potential field method is the effective methods to evaluate the cost of obstacles In the scene of suburban highways or expressways, the decline speed of the obstacles potential field in the l direction should be much greater than that in the s direction, so the ideal potential field shape of the obstacle should be an ellipse; When the relative speed between the obstacle and the vehicle is large, there is a higher risk of collision. Consequently, the potential obstacle field needs to consider the impact of the relative speed. Based on the above considerations, we choose the two-dimensional normal distribution function as the potential field function of the obstacle:

$$V_{obs} = \frac{C}{B\sigma_1\sigma_2\sqrt{8\pi^3}} \cdot \exp\left(-\frac{1}{2}\left(\frac{\left(s_g - s_{obs}\right)^2}{\sigma_1^2} + \frac{\left(l_g - l_{obs}\right)^2}{\sigma_2^2} + \frac{\left(\Delta v - v_{\Delta\max}\right)^2}{B^2}\right)\right) \tag{27}$$

where V_{obs} is the potential field value of the obstacle on a point in the sampling area; C is the obstacle influence coefficient; s_g and l_g are the s and l coordinates of a point in the sampling area; s_{obs} and l_{obs} are the s and l coordinates of the obstacle; Δv is the relative speed between the obstacle and the vehicle; $v_{\Delta max}$ is the relative speed of the static obstacle, and its value is equal to the current speed of the vehicle; B is the speed influence coefficient; σ_1, σ_2 are the shape parameters of the potential field in the s and l directions, in the normal distribution, $3\sigma_1$ and $3\sigma_2$ can represent the 0.9974 potential field shape information in the s and l directions. In our method, $3\sigma_1 = S_w$, S_w is the safe following vehicle distance, which can be found from Table 1, $3\sigma_2 = L_w$, L_w is the lane width.

According to (27), we can get the cost function of the forward obstacle and the lateral obstacle as:

$$F_{con} = \frac{C_1}{B\sigma_1\sigma_2\sqrt{8\pi^3}} \cdot \exp\left(-\frac{1}{2}\left(\frac{(s_g - s_{con})^2}{\sigma_1^2} + \frac{(l_g - l_{con})^2}{\sigma_2^2} + \frac{(\Delta v - v_{\Delta\,\max})^2}{B^2}\right)\right) \tag{28}$$

where F_{con} is the cost imposed by the forward obstacle on the point (s_g, l_g); C_1 is the influence coefficient of the forward obstacle.

$$F_{side} = \frac{C_2}{B\sigma_1\sigma_2\sqrt{8\pi^3}} \cdot \exp\left(-\frac{1}{2}\left(\frac{(s_g - s_{side})^2}{\sigma_1^2} + \frac{(l_g - l_{side})^2}{\sigma_2^2} + \frac{(\Delta v - v_{\Delta\,\max})^2}{B^2}\right)\right) \tag{29}$$

where F_{side} is the cost imposed by the lateral obstacle on the point (s_g, l_g); C_2 is the influence coefficient of the forward obstacle.

From (26)(28)(29), the obstacle cost function can be calculated by:

$$F_{obs} = F_{road} + F_{con} + \sum_{i=1}^{n} F_{side(i)} \tag{30}$$

where n is the number of lateral obstacles.

In the scene shown in Fig.13(a), the road cost function, the forward obstacle cost function and the lateral obstacle cost function in the sampling area are shown in Fig.13(b), Fig.13(c) and Fig.13(d).

2) COMFORT COST FUNCTION

Studies have shown that acceleration and jerk are among the main factors affecting driving comfort [29]. Considering that the planned path is a quintic spline curve, the acceleration can reflect the jerk. We use acceleration as the evaluation index of comfort.

The acceleration of a vehicle during driving mainly includes longitudinal acceleration, lateral acceleration and yaw acceleration. According to Yusof *et al.* [30], the human body is most sensitive to acceleration from the longitudinal and lateral directions and least sensitive to the yaw acceleration around the z-axis. Therefore, we establish a comfort cost function based on longitudinal acceleration and lateral acceleration.

The comfort cost function is shown in (31).

$$F_{cfort} = D \cdot \sqrt{a_{longaver}^2 + a_{lateraver}^2} \tag{31}$$

where D is the comfort influence coefficient; $a_{longaver}$ is the root-mean-square of the longitudinal acceleration, which is equal to the a_{long} in Section III; $a_{lateraver}$ is the root-mean-square of lateral acceleration, which can be calculated as (32)

$$a_{lateraver} = \begin{cases} \sqrt{\frac{1}{t_e}\left(\int_0^{t_e} (a_d + a_c)^2\right)}, & \text{sgn}(k_d) = \text{sgn}(k_c) \\ \sqrt{\frac{1}{t_e}\left(\int_0^{t_e} (a_d - a_c)^2\right)}, & \text{sgn}(k_d) \neq \text{sgn}(k_c) \end{cases} \tag{32}$$

where a_d is the offset lateral acceleration; a_c is the centripetal acceleration, respectively, which can be calculated by (8) and (11).

In the scene shown in Fig.13(a), the comfort cost function in the sampling area is shown in Fig.13(e).

3) ACCELERATION COST FUNCTION

In the traditional path planning method, the longitudinal speed of the vehicle when changing lanes or avoidance is constant. Due to the different speed limits between the carriageway and the overtaking lane, and the speed of obstacles in the lateral lane may not be the same as the speed of the vehicle, it is often necessary to accelerate or decelerate when changing lanes. Based on this, we design the acceleration cost function to plan the speed of the vehicle when changing lanes or avoidance according to the type of lane the vehicle drives after changing lanes and the obstacle information of the lateral lane.

In our method, the acceleration cost function is constructed based on a third-order polynomial, as shown in (33).

$$F_{acc} = E\left|s_g - sm\right|^3 \tag{33}$$

where F_{acc} is the acceleration cost function; E is the lane changing acceleration influence coefficient; sm is the zero cost s coordinate. When lane changing need to accelerate, sm takes the lateral lane upper boundary s_{22}, when lane changing need to decelerate, sm takes the lateral lane upper boundary s_{21}, based on the lane and lateral obstacle information, we design the lane-changing speed planning scheme as shown in Table 2

The acceleration cost function only acts on the road area in the vehicle's lateral movement direction.

In the scene shown in Fig.13(a), the acceleration cost function in the sampling area is shown in Fig.13(f).

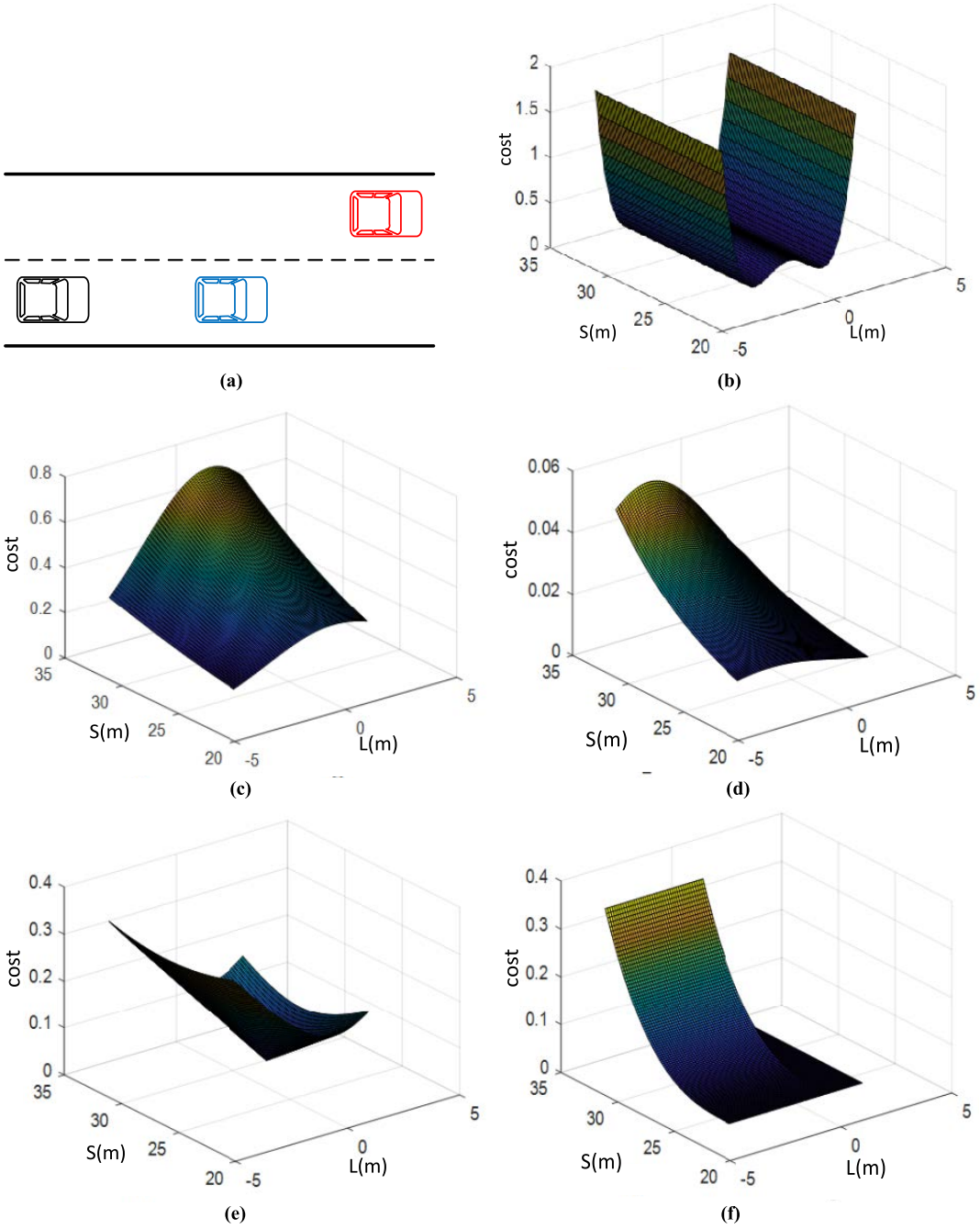

FIGURE 13. The distribution of the cost of different cost functions in the sampling area. (a) road scene, where black is the target vehicle, (b) the road cost function, (c) the forward obstacle cost function, (d)the lateral obstacle cost function, (e) the comfort cost function, (f) the acceleration cost function.

The total cost function shown by (34) is defined as the sum of the three cost functions.

$$\begin{cases} F_{side} = F_{obs} + F_{cfort} + F_{acc} \\ F_{fword} = F_{obs} + F_{cfort} \end{cases} \tag{34}$$

where F_{side} is the cost function of sampling points in the road area along the vehicle's lateral movement direction; F_{fwod} is the cost function of sampling points in the road area opposite to the vehicle's lateral movement direction.

B. OPTIMIZATION SOLUTION

In our method, we use quadratic programming to find the candidate points with the lowest cost. Since the cost function is non-linear. Therefore, the cost function needs to be transformed into a quadratic form through the Taylor formula.

We can gain equation (35) via the second-order Taylor expansion of equation (34).

$$Ff = F(s_{d0}, l_{d0}) + (s_d - s_{d0}) \cdot F'_{s_d}(s_{d0}, l_{d0})$$

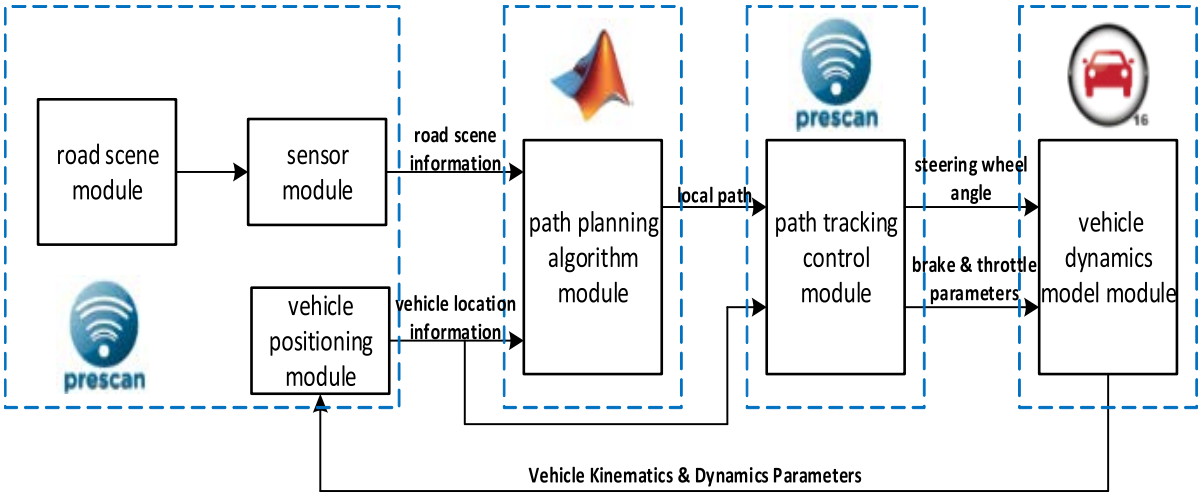

FIGURE 14. The framework of the co-simulation platform.

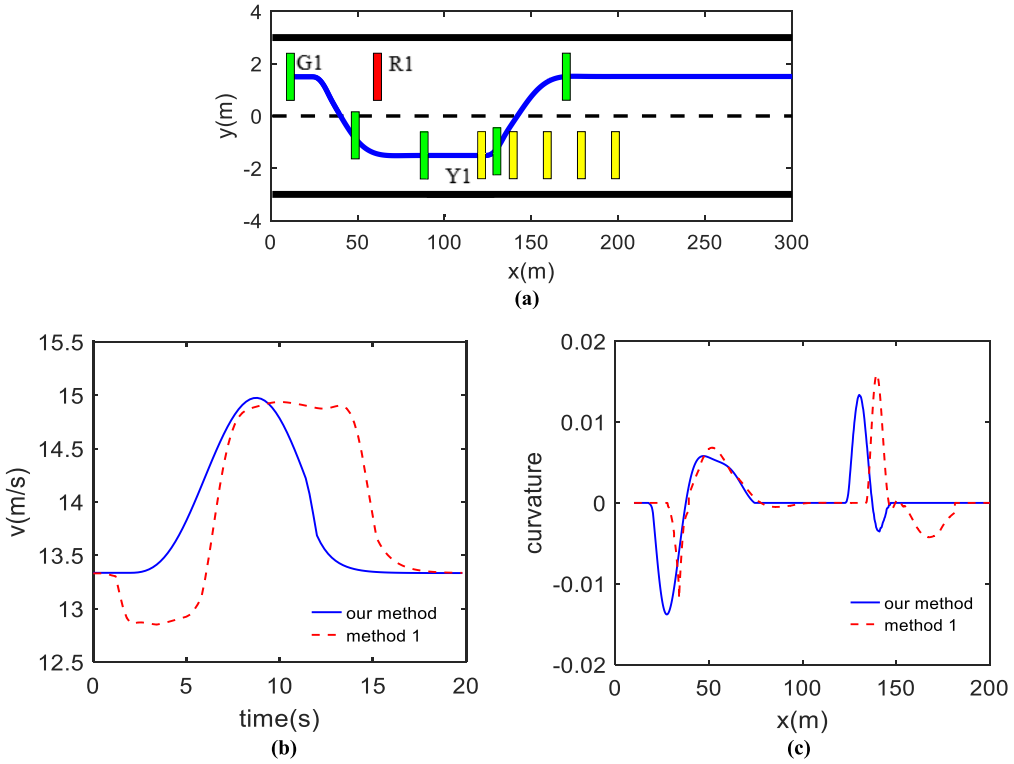

FIGURE 15. The vehicle continuously avoids two obstacles. (a) planning path and dynamic vehicle position, (b) speed comparison, (c) curvature comparison.

$$
\begin{aligned}
&+ (l_d - l_{d0}) \cdot F'_{l_d}(s_{d0}, l_{d0}) + \frac{1}{2!}(s_d - s_{d0})^2 \\
&\cdot F''_{s_d s_d}(s_{d0}, l_{d0}) + \frac{1}{2!}(s_d - s_{d0})(l_d - l_{d0}) \\
&\cdot F''_{s_d l_d}(s_{d0}, l_{d0}) + \frac{1}{2!}(s_d - s_{d0})(l_d - l_{d0}) \\
&\cdot F''_{l_d s_d}(s_{d0}, l_{d0}) + \frac{1}{2!}(l_d - l_{d0})^2 \\
&\cdot F''_{l_d l_d}(s_{d0}, l_{d0}) \qquad (35)
\end{aligned}
$$

where F is the total cost function; Ff is the quadratic form of the total cost function; s_{d0} and l_{d0} are the s coordinates and l coordinates of any point within the boundary conditions.

Arranging (35), the standard quadratic form of Ff is described as:

$$Ff = As_d^2 + Bl_d^2 + Cs_d l_d + D \qquad (36)$$

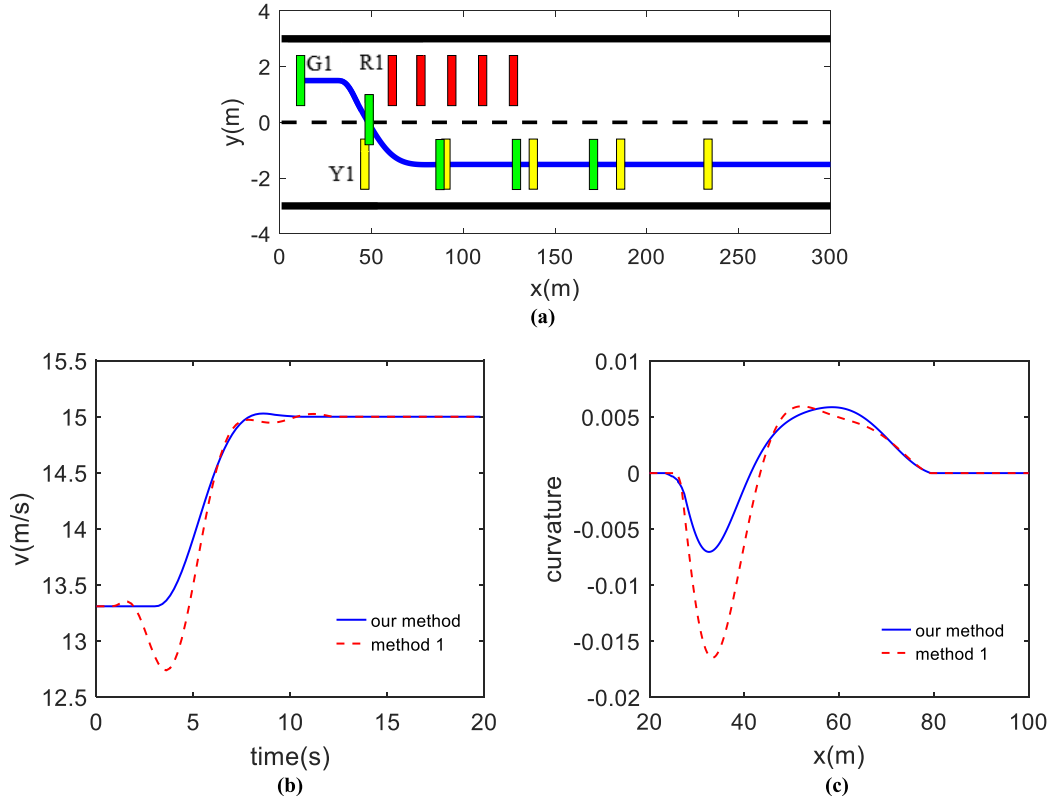

FIGURE 16. The vehicle directly changing lane to avoid obstacles under the straight road (a) planning path and vehicle dynamic position, (b) speed comparison, (c) curvature comparison.

The mathematical model of quadratic programming can be expressed as:

$$\begin{cases} \min f\ (X) = \sum_{j=1}^{n} c_j x_j + \frac{1}{2} \sum_{j=1}^{n} \sum_{k=1}^{n} c_{jk} x_j x_k \\ c_{jk} = c_{kj}, \quad k = 1, 2, \cdots, n \\ \sum_{j=1}^{n} a_{ij} x_j + b_i \geq 0, \quad i = 1, 2, \cdots, m \\ x_j \geq 0, \quad j = 1, 2, \cdots, n \end{cases} \tag{37}$$

Since the side lanes and the forward lanes have different boundary conditions, the sampling area needs to be quadratically programmed according to $l > 0$m and $l < 0$m.

In order to ensure that the quadratic programming is carried out in the convex space, it is necessary to assign the initial values s_{d0} and l_{d0}. The initial value can be obtained by calculating the minimum value of the sampling point in the sampling area $l > 0$m and $l < 0$m respectively by using the (34), which can be used as the initial input of the quadratic programming.

Introducing forward obstacle boundary conditions and obstacle boundary conditions according to (25), the candidate point with the smallest cost value of the forward lane $F_{fword\min}$ ($P_{fword\min}$), coordinates $P_{fword\min}$ ($s_{fword\min}$, $l_{fword\min}$), and lateral lane $F_{side\min}$($P_{side\min}$), coordinates $P_{side\min}$($s_{side\min}$, $l_{side\min}$) can be calculated by eq. (37).

The optimal candidate point $P_{\min}(s_{\min}, l_{\min})$ can be obtained by:

$$\begin{cases} P_{\min} = P_{frond\,\min}, & F_{frond\,\min} < F_{side\,\min} \\ P_{\min} = P_{side\,\min}, & F_{frond\,\min} > F_{side\,\min} \end{cases} \tag{38}$$

C. PLANNING PATH ENGENDERER

The planned path should meet the following two requirements:

1. When the vehicle drives along the path, the yaw angle, lateral speed and lateral acceleration should be continuous.

2. A path can be uniquely determined when the state of the start and end of the path is known.

Our method samples the quintic spline curve to generate the path, which meets the above two requirements and has the merits of simplicity, efficiency, and adaptability.

The path that conforms to the quintic spline curve should satisfy:

$$\begin{cases} l = at^5 + bt^4 + ct^3 + dt^2 + et + f \\ s = \frac{1}{2} a_s t^2 + v_0 t + g \end{cases} \tag{39}$$

where $a \sim g$ are undetermined coefficients; a_s is the average longitudinal acceleration, which can be described as:

$$a_s = \frac{1}{2} \left(\frac{1}{2} \left(s_{d\,\min} - s_s \right) - v_0 \right) \tag{40}$$

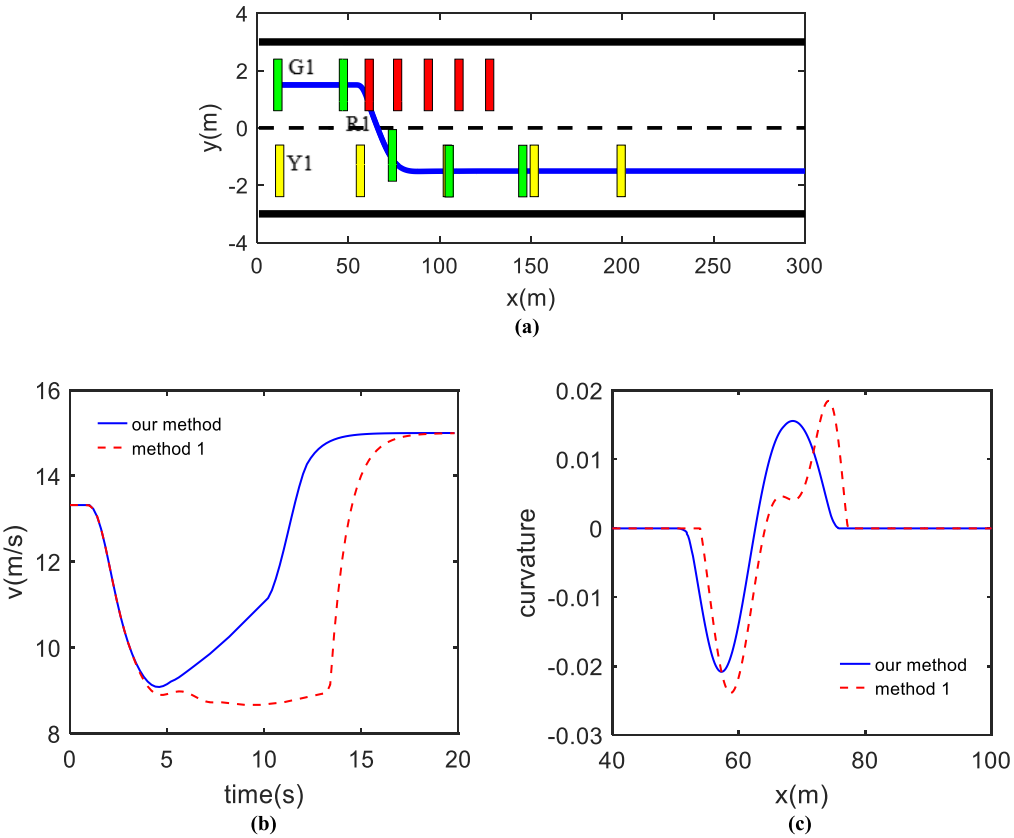

FIGURE 17. The obstacles before changing lanes under the straight road (a) planning path and vehicle dynamic position, (b) speed comparison, (c) curvature comparison.

According to the state of the start and end of the path, boundary conditions can be obtained as:

$$\begin{cases} l(0) = l_s, \quad \dot{l}(0) = v_{ls}, \quad \ddot{l}(0) = a_{ls} \\ l(t_e) = l_{g\min}, \quad \dot{l}(t_e) = 0, \quad \ddot{l}(0) = 0 \\ s(0) = s_s, \quad s(t_e) = s_{g\min} \end{cases} \tag{41}$$

where $l_{g\min}$ and $s_{g\min}$ are the $s-l$ coordinates of the optimal point. Simultaneous (40) (41), we can solve the undetermined coefficients $a \sim g$.

V. SIMULATION RESULTS

In order to comprehensively and reliably verify the feasibility and effectiveness of the dynamic path planning method in this paper, we built a co-simulation platform based on Prescan, Matlab/Simulink and Carsim. Prescan provides vehicle positioning information, road scene information and a path follower with preview. The road scene information is obtained by the AIR sensor and Lane Marker sensor provided by Prescan. Both the AIR sensor and the Lane Marker sensor are truth sensors without error; based on the path follower with preview as the default path tracing controller in Precan. Matlab/Simulink is used to write the path planning method and visualize the results of the simulation. Carsim provides vehicle dynamics models that can be imported from Prescan's third-party model library. The framework of the co-simulation platform is shown in Fig.14. Based on the above co-simulation platform, we designed different scenarios to verify the method Simulation scenes include straight road scenes and s-bend scenes that are common in suburban roads and expressways.

In Fig. 15-18, the solid black line indicates the road boundary line, the black dashed line indicates the lane line, the blue line indicates the planned path. For aesthetics, we set the vehicles and obstacles as rectangles in the straight road scene and set the vehicles and obstacles as circles in the s-bend scene green indicates the vehicle; red indicates obstacles on the carriageway; yellow indicates obstacle on the overtaking lane.

In order to express the effectiveness of the path planning method in dynamic scenes, we show the relative position of each obstacle and the vehicle at the exact moment in time sequence in the simulation. The straight road scene is shown in Fig. 15∼17, G1, R1, Y1 indicate the vehicle's initial position, obstacles in the carriageway, and obstacles in the overtaking lane. After that, the position of the vehicle and the obstacle are recorded every 2.5s. The s-bend scene is shown in Fig.18. G,R, and Y represent the initial avoidance positions of the vehicle, obstacles in the driving lane, and obstacles in the overtaking lane, respectively. The positions of the vehicle and obstacles are recorded every 1s.

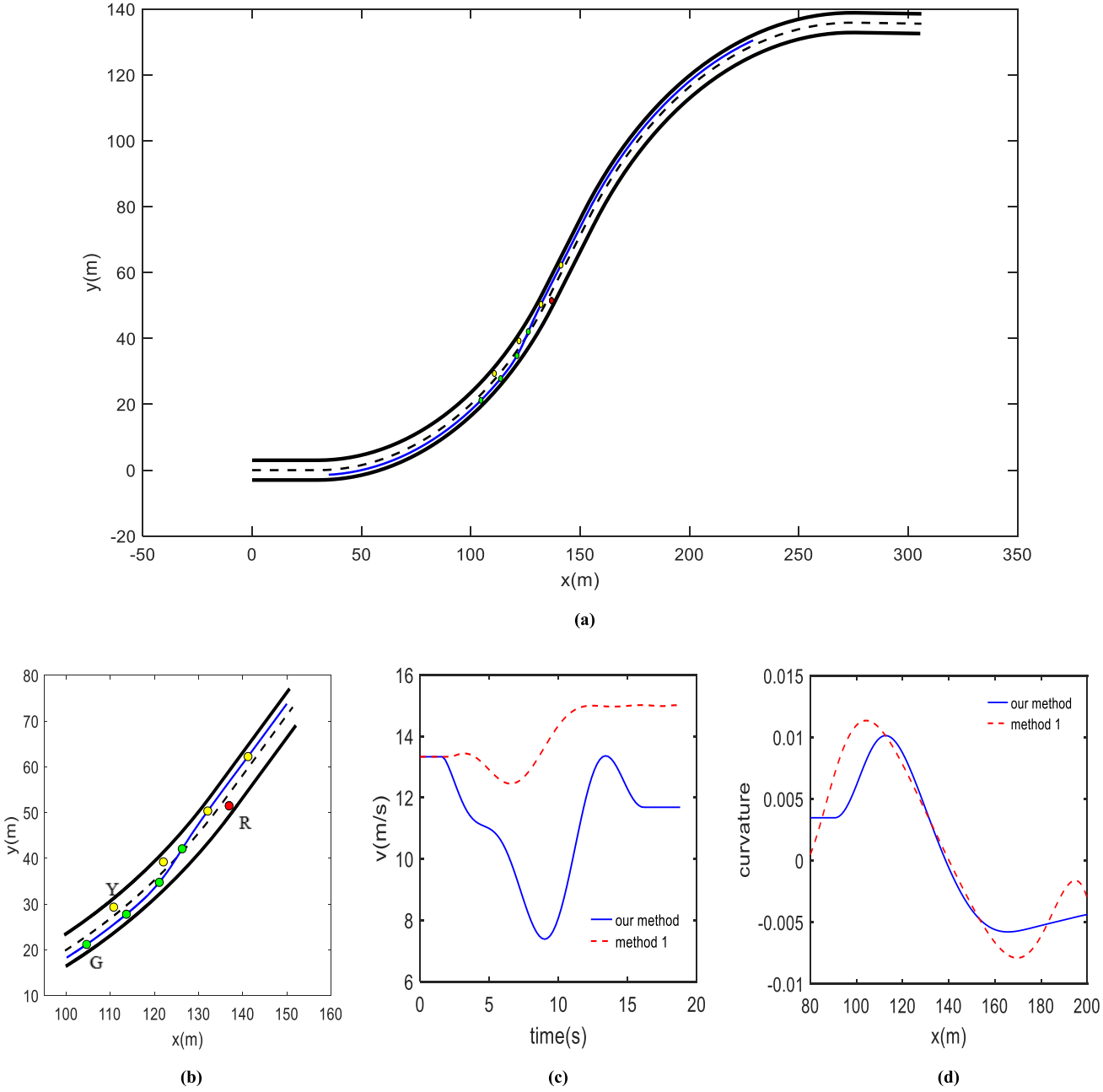

FIGURE 18. The vehicle avoiding the dynamic obstacles on an s-bend road. (a) planning complete path map, (b) local map of the planning path and dynamic vehicle position, (c) speed comparison, (d) curvature comparison.

In addition, we also further illustrate the advantages of our method by comparing the speed and trajectory curvature with the dynamic path planning method base on path discrete mentioned in the reference [15] (called method 1) in the scenario of Figure 15-18.

A. STRAIGHT ROAD SCENE

1) STRAIGHT ROAD CONTINUOUS AVOIDANCE

Fig.15 is a driving scene where the vehicle continuously avoids two obstacles. In Fig.15, the carriageway obstacle R is a static obstacle, the initial position $x_{R1} = 60$m; the overtaking lane obstacle Y is a dynamic obstacle, the initial position $x_{Y1} = 120$m, and it is driving at a constant speed of 9m/s^2. As shown in Fig.15 (a) and the solid blue line in Fig.15(b), after detecting obstacle R, the vehicle accelerates to the overtaking lane to avoid obstacles and successfully drove into the centre of the overtaking lane; After driving for a certain distance in the overtaking lane, the vehicle detects the dynamic obstacle Y, it decelerates to the carriageway to avoid obstacles, and continue to decelerate to

cruising speed after successfully entering the centre of the carriageway.

Fig.15(b)(c) shows the comparison between method 1 and our method in velocity and trajectory curvature, where the red dotted line represents method 1. From the fig.15(b)(c), we can see that method 1 decelerates when the vehicle avoids the first obstacle, which makes the speed fluctuate significantly during the lane change process, and it takes a longer time to complete the continuous avoidance of two obstacles. In addition, our method has less fluctuation in trajectory curvature, which means that the path obtained using our method is smoother than that of method 1

2) STRAIGHT ROAD DIRECT LANE CHANGING AVOID–ANCE

In the driving scene shown shown in Fig.16, the vehicle is directly changing lane to avoid obstacles under the straight road, where both the carriageway obstacle R and the overtaking lane obstacle Y are dynamic obstacles. The initial position of obstacle R is $x_{R1} = 60$m, and driving at a constant speed of 8m/s^2; the initial position of obstacle Y is $x_{Y1} = 45$m and driving at a constant speed of 16m/s^2. As shown in Fig.16(a), since the overtaking lane meets the lateral obstacle boundary conditions and has a lower cost, the vehicle will directly change lanes to avoid obstacles after detecting the obstacle R.

Figure 16(b)(c) shows the speed comparison and trajectory curvature comparison between method 1 and our method in the direct lane changing avoidance scene From the figure, we can see that method 1 has an obvious deceleration process when the vehicle changes lanes, while in our method, the vehicle will continue to accelerate during the lane changing process, which reduces the parallel time between the vehicle and the obstacle R and improves lane changing safety. Our method also had smaller curvature fluctuations compared to method 1.

3) STRAIGHT ROAD UNIQUE SCENE AVOIDANCE

In the scene shown in Fig.17, the initial position of the carriageway obstacle R is $x_{R1} = 60$m, and driving at a constant speed of 8m/s^2, and initial position of the overtaking lane obstacle Y is $x_Y1 = 10$m and driving at a constant speed of 16m/s^2. As shown in Fig.17 (a) and the solid blue line in Fig.17(b), in this scene, because the overtaking lane does not meet the lateral obstacle boundary conditions, the vehicle cannot avoid obstacle R by changing lanes directly. Consequently, the vehicle first decelerates and follows the obstacle R drive until the passing lane meets the lateral obstacle boundary conditions and has a lower cost.

In Fig.17(b)(c), comparing the speed and trajectory curvature of method 1 with our method, we can see that method 1 takes longer time to follow the obstacle R. Compared with method 1, our method obviously has higher efficiency and can quickly change lanes to avoid obstacles after the lateral lanes meets the lateral obstacle boundary conditions and has a lower cost. In addition, our method has better trajectory curvature smoothness than method 1.

B. S-BEND SCENE

Fig.18 is a driving scene of the vehicle avoiding the static obstacle R when there is a dynamic obstacle Y in the overtaking lane on the s- bend road. In Fig.18, the dynamic obstacle Y drives in the overtaking lane at a speed of 15m/s^2. As shown in Fig.18 (a) (b) and the solid blue line in Fig.18(c), when the vehicle detects the obstacle R, the overtaking lane does not meet the lateral obstacle boundary conditions due to the influence of the obstacle Y, so the vehicle decelerates until the overtaking lane meets lateral obstacle boundary conditions. In addition, due to the large curvature of the bend in the scene shown in Fig.18, the cruising speed after the vehicle enters the bend is lower than the cruising speed on the straight road.

The speed comparison and trajectory curvature comparison between method 1 and our method in the S-bend scene are shown in Fig.18(c)(d). From the figure, we can see that since the curvature speed limit is not considered, method 1 does not reduce the cruising speed after the vehicle enters the bend, which may cause the vehicle to become unstable. In addition, the curvature of the trajectory obtained by method 1 fluctuates greatly, and the smoothness of the path is worse than our method.

VI. CONCLUSION

This paper designs a dynamic path planning method based on discrete optimization which use in suburban highways or expressways. This method uses the quadratic planning method to find the optimal candidate points in the $s - l$ coordinate system according to different driving conditions, and connects the initial position of the vehicle with the candidate points to generate a path through a quintic spline curve. In order to make the planned path meet the requirements of safety, comfort and real-time, considering the kinematics and obstacle boundary conditions, a two-dimensional normal distribution obstacle cost function based on the potential field, comfort cost function and acceleration cost function of the decision-making obstacle avoidance speed are designed, allows the planned path avoid stationary and moving obstacles effectively under various driving conditions.

The simulation results show that the method can plan a safe and comfortable path with appropriate speed to guide the vehicle to avoid dynamic and static obstacles in straight and curved scenes. It can be widely used in the local path planning of autonomous vehicles in suburban highways or expressways, but in the case of urban roads with more complex environments and more urgent driving conditions, more complete and radical discrete methods and cost functions need to be designed.

REFERENCES

[1] J. Ni and J. Hu, "Dynamics control of autonomous vehicle at driving limits and experiment on an autonomous formula racing car," *Mech. Syst. Signal Process.*, vol. 90, pp. 154–174, Jun. 2017.

[2] A. K. Tyagi and S. U. Aswathy, "Autonomous intelligent vehicles (AIV): Research statements, open issues, challenges and road for future," *Int. J. Intell. Netw.*, vol. 2, pp. 83–102, Jan. 2021.

[3] S. Pendleton, H. Andersen, X. Du, X. Shen, M. Meghjani, Y. Eng, D. Rus, and M. Ang, "Perception, planning, control, and coordination for autonomous vehicles," *Machines*, vol. 5, no. 1, p. 6, Feb. 2017.
[4] B. Song, Z. Wang, L. Zou, L. Xu, and F. E. Alsaadi, "A new approach to smooth global path planning of mobile robots with kinematic constraints," *Int. J. Mach. Learn. Cybern.*, vol. 10, no. 1, pp. 107–119, Jan. 2019.
[5] S. Dixit, S. Fallah, U. Montanaro, M. Dianati, A. Stevens, F. Mccullough, and A. Mouzakitis, "Trajectory planning and tracking for autonomous overtaking: State-of-the-art and future prospects," *Annu. Rev. Control*, vol. 45, pp. 76–86, Jan. 2018.
[6] P. Marin-Plaza, A. Hussein, D. Martin, and A. D. L. Escalera, "Global and local path planning study in a ROS-based research platform for autonomous vehicles," *J. Adv. Transp.*, vol. 2018, pp. 1–10, Feb. 2018.
[7] G. Tang, C. Tang, C. Claramunt, X. Hu, and P. Zhou, "Geometric A-star algorithm: An improved A-star algorithm for AGV path planning in a port environment," *IEEE Access*, vol. 9, pp. 59196–59210, 2021.
[8] D. Ferguson, T. M. Howard, and M. Likhachev, "Motion planning in urban environments," *J. Field Robot.*, vol. 25, nos. 11–12, pp. 939–960, Nov. 2008.
[9] U. Orozco-Rosas, O. Montiel, and R. Sepúlveda, "Mobile robot path planning using membrane evolutionary artificial potential field," *Appl. Soft Comput. J.*, vol. 77, pp. 236–251, Apr. 2019.
[10] E. Wu, Y. Sun, J. Huang, C. Zhang, and Z. Li, "Multi UAV cluster control method based on virtual core in improved artificial potential field," *IEEE Access*, vol. 8, pp. 131647–131661, 2020.
[11] X.-D. Zhang, *A Matrix Algebra Approach to Artificial Intelligence*, 2020, p. 803.
[12] X. Zhao, S. Ding, Y. An, and W. Jia, "Asynchronous reinforcement learning algorithms for solving discrete space path planning problems," *Int. J. Speech Technol.*, vol. 48, no. 12, pp. 4889–4904, Dec. 2018.
[13] B. Kim and J. Pineau, "Socially adaptive path planning in human environments using inverse reinforcement learning," *Int. J. Social Robot.*, vol. 8, no. 1, pp. 51–66, Jan. 2016.
[14] C. Katrakazas, M. Quddus, W.-H. Chen, and L. Deka, "Real-time motion planning methods for autonomous on-road driving: State-of-the-art and future research directions," *Transp. Res. C, Emerg. Technol.*, vol. 60, pp. 416–442, Nov. 2015.
[15] H. Fan, F. Zhu, C. Liu, L. Zhang, L. Zhuang, D. Li, W. Zhu, J. Hu, H. Li, and Q. Kong, "Baidu Apollo EM motion planner," 2018, *arXiv:1807.08048*.
[16] K. Bergman, O. Ljungqvist, and D. Axehill, "Improved path planning by tightly combining lattice-based path planning and optimal control," *IEEE Trans. Intell. Vehicles*, vol. 6, no. 1, pp. 57–66, Mar. 2021.
[17] D. Feng, L. Deng, T. Sun, H. Liu, H. Zhang, and Y. Zhao, "Local path planning based on an improved dynamic window approach in ROS," in *Proc. Int. Conf. Comput. Eng. Netw.* Singapore: Springer, 2020, pp. 1164–1171.
[18] Y. Jiang, X. Jin, Y. Xiong, and Z. Liu, "A dynamic motion planning framework for autonomous driving in urban environments," in *Proc. 39th Chin. Control Conf. (CCC)*, Jul. 2020, pp. 5429–5435.
[19] X. Hu, L. Chen, B. Tang, D. Cao, and H. Hee, "Dynamic path planning for autonomous driving on various roads with avoidance of static and moving obstacles," *Mech. Syst. Signal Process.*, vol. 100, pp. 482–500, Feb. 2018.
[20] C. Zhang, D. Chu, S. Liu, Z. Deng, C. Wu, and X. Su, "Trajectory planning and tracking for autonomous vehicle based on state lattice and model predictive control," *IEEE Intell. Transp. Syst. Mag.*, vol. 11, no. 2, pp. 29–40, Summer 2019.
[21] K. Chu, M. Lee, and M. Sunwoo, "Local path planning for off-road autonomous driving with avoidance of static obstacles," *IEEE Trans. Intell. Transp. Syst.*, vol. 13, no. 4, pp. 1599–1616, Dec. 2012.
[22] Y. Meng, Y. Wu, Q. Gu, and L. Liu, "A decoupled trajectory planning framework based on the integration of lattice searching and convex optimization," *IEEE Access*, vol. 7, pp. 130530–130551, 2019.
[23] Z. Chen, Y. Zhang, Y. Zhang, Y. Nie, J. Tang, and S. Zhu, "A hybrid path planning algorithm for unmanned surface vehicles in complex environment with dynamic obstacles," *IEEE Access*, vol. 7, pp. 126439–126449, 2019.
[24] T. H. Yimer, C. Wen, X. Yu, and C. Jiang, "A study of the minimum safe distance between human driven and driverless cars using safe distance model," 2020, *arXiv:2006.07022*.
[25] D. Chindamo, B. Lenzo, and M. Gadola, "On the vehicle sideslip angle estimation: A literature review of methods, models, and innovations," *Appl. Sci.*, vol. 8, no. 3, p. 355, 2018.
[26] Y. Zhang, H. Chen, S. L. Waslander, T. Yang, S. Zhang, G. Xiong, and K. Liu, "Speed planning for autonomous driving via convex optimization," in *Proc. 21st Int. Conf. Intell. Transp. Syst. (ITSC)*, Nov. 2018, pp. 1089–1094.
[27] T. Kuroda, "Simulation of generation and development of traffic jam in sag zone," *Trans. Jpn. Soc. Comput. Methods Eng.*, vol. 8, no. 11, 2008, Art. no. 081128.
[28] Q. Tu, H. Chen, and J. Li, "A potential field based lateral planning method for autonomous vehicles," *SAE Int. J. Passenger Cars-Electron. Elect. Syst.*, vol. 10, no. 1, pp. 24–35, 2017.
[29] A. Thatcher, "Green ergonomics: Definition and scope," *Ergonomics*, vol. 56, no. 3, pp. 389–398, Mar. 2013.
[30] N. M. Yusof, J. Karjanto, J. Terken, F. Delbressine, M. Z. Hassan, and M. Rauterberg, "The exploration of autonomous vehicle driving styles: Preferred longitudinal, lateral, and vertical accelerations," in *Proc. 8th Int. Conf. Automot. User Interfaces Interact. Veh. Appl.*, Oct. 2016, pp. 245–252.

HAOBIN JIANG received the B.S. degree in agricultural mechanization from Nanjing Agricultural University, Nanjing, China, in 1991, and the M.S. and Ph.D. degrees in vehicle engineering from Jiangsu University, Zhenjiang, China, in 1994 and 2000, respectively. From 1994 to 1995, he was a Research Assistant with the Laboratory of Power and Energy, Faculty of Biological Resources, Mie University, Mie, Japan. He joined Jiangsu University in 1994, where he is currently a Professor of vehicle engineering. His research interests include vehicle dynamic performance analysis and electrical control technology, active safety control techniques and theories of road vehicles, and intelligent transportation technology. He is the Steering Technology Committee Member of the Society of Automotive Engineering of China, the Steering Technology Committee Member of the National Technical Committee of Auto Standardization of China, and the Standing Director of the Society of Automotive Engineering of Jiangsu.

JIAN PI received the B.S. degree in vehicle engineering from Jiangsu University, Zhenjiang, China, in 2019, where he is currently pursuing the M.S. degree with the Department of Vehicle Engineering. His research interests include path planning and intelligent vehicle.

AOXUE LI received the B.S., M.S., and Ph.D. degrees in vehicle engineering from Jiangsu University, Zhenjiang, China, in 2013, 2016, and 2020, respectively. From August 2018 to August 2019, he was a Visiting Scholar with the Department of Mechanical Engineering, Michigan State University, East Lansing, MI, USA. He is currently a Lecturer with the School of Automotive and Traffic Engineering, Jiangsu University. His research interests include autonomous vehicle, intelligent transportation systems, and ADAS technologies.

CHENHUI YIN received the B.S. degree in vehicle engineering and the M.S. degree in traffic and transportation engineering from Jiangsu University, Zhenjiang, China, in 2016 and 2019, respectively, where he is currently pursuing the Ph.D. degree. He is also a Ph.D. Researcher at Cranfield University, Bedford, U.K. His research interests include human–like decision making and trajectory planning of autonomous vehicles, and control and optimization of commercial vehicle intelligent hybrid power steering systems.